Heliyon 9 (2023) e22279

Contents lists available at ScienceDirect

Heliyon

journal homepage: www.cell.com/heliyon

Characterization and *in vivo* evaluation of a fabricated absorbable poly(vinyl alcohol)-based hernia mesh

Erfan Dorkhani [a,b], Bahareh Darzi [a,b,1], Laleh Foroutani [a,c,1], Zahra Ebrahim Soltani [d], Seyed Mohsen Ahmadi Tafti [a,c,*]

[a] *Research Center for Advanced Technologies in Cardiovascular Medicine, Cardiovascular Diseases Research Institute, Tehran University of Medical Sciences, Tehran 1411713138, Iran*
[b] *School of Chemical Engineering, College of Engineering, University of Tehran, Tehran 1417614411, Iran*
[c] *Colorectal Research Center, Imam Khomeini Hospital Complex, Tehran University of Medical Sciences, Tehran 1419733141, Iran*
[d] *Experimental Medicine Research Center, Tehran University of Medical Sciences, Tehran, Iran*

ARTICLE INFO

Keywords:
Hernia repair
poly(vinyl alcohol)
Solution casting
Zinc oxide nanoparticles
Citric acid
Freeze-thaw

ABSTRACT

The most widely taken medical approach toward hernia repair involves the implementation of a prosthetic mesh to cover the herniated site and reinforce the weakened area of the abdominal wall. Biodegradable meshes can serve as biocompatible grafts with a low risk of infection. However, their major complication is associated with a high rate of degradation and hernia recurrence. We proposed a facile and cost-effective method to fabricate a poly(vinyl alcohol)-based mesh, using the solution casting technique. The inclusion of zinc oxide nanoparticles, citric acid, and three cycles of freeze-thaw were intended to ameliorate the mechanical properties of poly(vinyl alcohol). Several characterization, cell culture, and animal studies were conducted. Swelling and water contact angle measurements confirmed good water uptake capacity and wetting behavior of the final mesh sample. The synthesized mesh acquired a high mechanical strength of 52.8 MPa, and its weight loss was decreased to 39 %. No cytotoxicity was found in all samples. *In vivo* experiments revealed that less adhesion and granuloma formation, greater tissue integration, and notably higher neovascularization rate were resulted from implanting this fabricated hernia mesh, compared to commercial Prolene® mesh. Furthermore, the amount of collagen deposition and influential growth factors were enhanced when rats were treated with the proposed mesh instead of Prolene®.

1. Introduction

A hernia occurs when an internal organ protrudes or prolapses through a weak spot in the cavity that encircles it [1]. Groin and ventral hernias are two major categories of hernias, each comprises of several subdivisions. These types of hernias are sorted based on their anatomical location in the abdominal wall, which is the most vulnerable site to herniation [2,3]. Several risk factors are known to contribute to this disorder, such as genetics, obesity, pregnancy, constipation, heavy lifting, and physical activity.

* Corresponding author. Colorectal Research Center, Imam Khomeini Hospital Complex, Tehran University of Medical Sciences, Tehran 1419733141, Iran.
E-mail address: smahmadit@sina.tums.ac.ir (S.M. Ahmadi Tafti).
[1] These authors contributed equally to this work.

https://doi.org/10.1016/j.heliyon.2023.e22279
Received 21 December 2022; Received in revised form 7 November 2023; Accepted 8 November 2023
Available online 15 November 2023

List of Abbreviations

WAW	Watch-and-wait
PP	Polypropylene
PVA	Poly(vinyl alcohol)
ZnO NPs	Zinc oxide nanoparticles
CA	Citric acid
PX	Physical crosslinking
PBS	Phosphate-buffered saline
DMEM	Dulbecco's Modified Eagle Medium
DMSO	Dimethyl sulfoxide
BSA	Bovine serum albumin
MTT	3-(4,5-dimethylthiazol-2-yl)-2,5-diphenyltetrazolium bromide
FT-IR	Fourier transform infrared spectroscopy
ATR	Attenuated total reflection
SEM	Scanning electron microscopy
FEG	Field emission gun
WCA	Water contact angle
IP	Intraperitoneal
H&E	Hematoxylin and eosin
SPSS	Statistical package for social sciences
STD	Standard deviation
ECM	Extracellular matrix
MT	Masson's Trichrome
TGF-β	Transforming growth factor beta
IHC	Immunohistochemistry
PDGF	Platelet-derived growth factor

The approach to hernia treatment normally contains watch-and-wait (WAW) for mild cases and surgical intervention (also known as hernia repair) for severe ones [4]. Hernia repair can be performed through direct suture repair, suggested to become extinct due to significant recurrence rates [5], or implantation of a polymeric mesh via open repair or laparoscopic surgery. While laparoscopic surgery is a minimally invasive approach, conventional (open) surgery involves making an incision over the hernia site and pushing the hernia back into the abdominal cavity. Various means of fixation, such as tacks, glues, staples, or sutures are known to keep the mesh in its correct position until complete closure of the defect is achieved [6].

As opposed to suture repair, with the insertion of a mesh, tension-free restoration and facilitated incorporation into the host tissue can be achieved, resulting in a decreased recurrence rate [7]. Reported by Burger et al. [5], during a median follow-up of 81 months, recurrence rates were halved when mesh was used instead of the suture. In addition, Burati et al. [6] stated the possibility of reducing recurrence rates to below 5 % with an appropriate choice of surgical mesh and fixation method.

Wang See et al. [4] classified 70–80 types of commercially available hernia meshes into three categories based on the materials of construction: Synthetic, biological, and composite. As the most frequent type of mesh used in clinical practice, synthetic meshes can be either non-absorbable (permanent) or absorbable (biodegradable). Polypropylene (PP, Prolene®) is a non-absorbable mesh with high popularity due to its inexpensiveness, excellent mechanical support and good tissue integration [8], however, because of the long-term durability and strong mechanical properties, this subset of synthetic mesh is associated with adhesion, erosion, chronic pain, and fistula formation. Moreover, it may restrict body movements and require a secondary operation to remove the mesh [9,10]. Absorbable mesh grafts on the other hand, cause less inflammation, but their short-term mechanical stability leads to hernia recurrence [11,12]. Sanders and Kingsnorth [13] introduced various features of an ideal prosthetic mesh, however, none of the currently available meshes obtains these characteristics all together. This study aimed to fabricate a biocompatible, non-adhesive mesh with appropriate strength and elasticity to lower the recurrence rate of herniation and even achieve controlled drug release in future studies.

Poly(vinyl alcohol) (PVA) is a biocompatible and biodegradable polymer, proven to provide excellent tissue integration with no cytotoxicity [14]. Several studies have evaluated the application of different PVA-based meshes for hernia repair: Fehér et al. and Molnár et al. fabricated electrospun PVA scaffolds with different concentrations and crosslinking methods. They both reported that these implants can serve as biocompatible meshes with minimal inflammatory response and adhesion to intra-abdominal tissue, as well as good integration [15,16]. The research group of Voniatis et al. [17] proved that fibrous polysuccinimide/PVA composites have favorable mechanical properties, while enhancing cell proliferation with no cytotoxicity. In another research of Fehér et al. [14], it was shown that after a long-term contact, only about 30 % of the adhesions resulted from the PVA mesh and minor inflammation was also reported. Shin et al. [18] synthesized a phosphate crosslinked PVA mesh using 3D printing technology. This bioscaffold could function as an inflammation trap, and reduce the formation of visceral adhesions. The mechanical properties of the mesh were also optimized by changing printing parameters. To further reduce post-operative infections, the incorporation of antimicrobial agents in surgical meshes has been gaining increasing attention [19]. A bifunctional composite mesh with a PP backbone and two different sides was fabricated

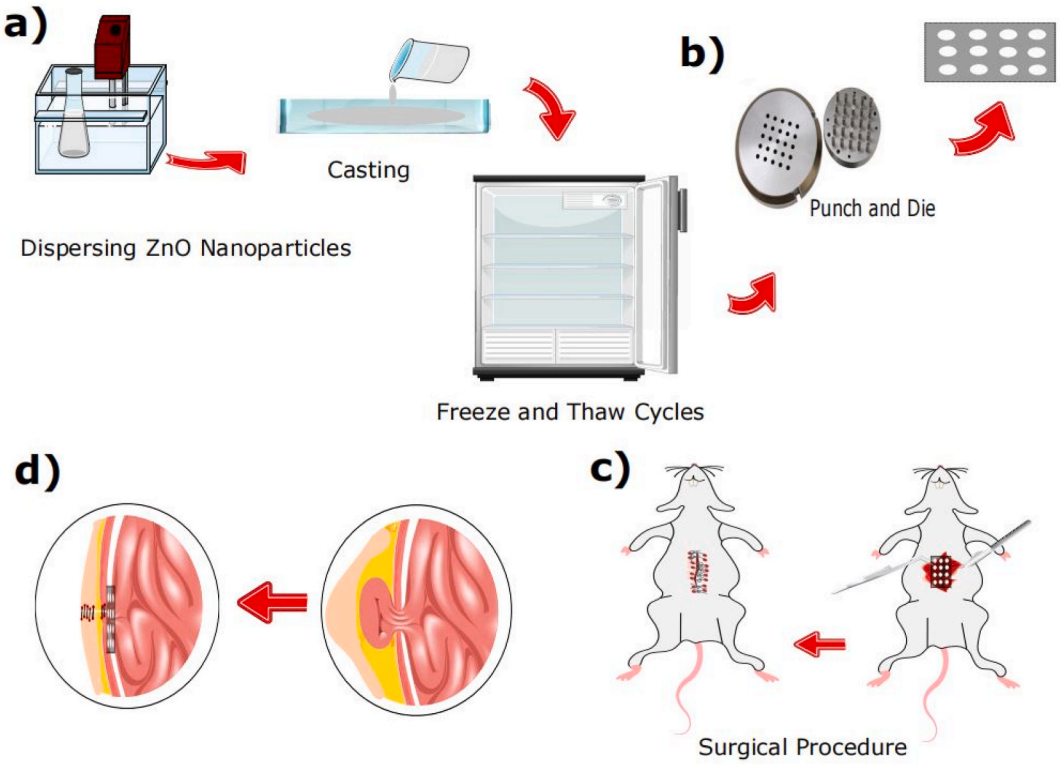

Fig. 1. Schematic illustration of (a) fabrication procedure of the modified PVA mesh graft based on solution casting technique: an ultrasonic bath was used to homogenize ZnO NPs dispersion. After casting the final PVA-ZnO-CA solution into the 10 × 10 cm^2 mold, physical crosslinking was achieved by three repeats of freezing (for 12 h at −20 °C) and thawing (for 8 h at 24 °C); (b) creation of mesh pores using a self-made punch and die, resulting in uniform and well-arranged circular holes in the mesh; (c) creation of a defect in the abdominal wall in an animal model, placement and fixation of the mesh using single interrupted sutures, and finally stitching the skin incision; (d) protrusion of a small part of the intestine (right) and treatment of the herniated site by the implementation of a surgical mesh (left).

through the work of Shokrollahi et al. [20]. The front side, containing ofloxacin drug and PVA fibers, showed good anti-adhesion performance and antibacterial effect, while the back side acted as a mesh fixer to the abdominal wall. In another study [21], 3D printed PP and PVA mesh incorporated with ciprofloxacin were prepared. Faster wound healing, as well as no signs of inflammation and adhesion were observed for drug-loaded PVA.

Mesh fabrication techniques mainly comprise knitting, weaving, and 3D printing. These structures were defined in the literature [2, 22]. Compared to woven meshes, knitted ones are more porous and more flexible, but weaker. In addition, the woven configuration has the disadvantage of insufficient integration with host tissue [4]. 3D printing, is a next-generation technology capable of producing accurate, patient-specific meshes by allowing to fine-tune several features. However, this approach is expensive, requires more investigation, and lacks the elasticity to properly respond to abdominal pressure [23]. Solution casting is one of the oldest and most straightforward techniques of film preparation, based on dissolving soluble polymers in water, followed by casting in a Petri dish or a mold [24,25].

In this study, we proposed a facile and cost-effective method based on solution casting to synthesize surgical meshes. To further diminish adhesiveness, and improve mechanical support and degradation period of PVA polymer, three modifications were performed: Addition of zinc oxide nanoparticles (ZnO NPs), incorporation of citric acid (CA) as a chemical crosslinker, and application of three cycles of freeze-thaw as physical crosslinking (PX). It should be mentioned that ZnO NPs function as antimicrobial agents, as well. Studied by Abdeen et al. [26], loading ZnO NPs on chitosan/PVA polymer significantly increased antimicrobial activity. Both ZnO and CA benefit from availability, inexpensiveness, and no cytotoxicity [9,27]. In addition to characterization and *in vitro* studies, we conducted *in vivo* experiments using a small animal model to evaluate the potential of the PVA-ZnO-PX-CA mesh in biomedical applications.

2. Materials and methods

2.1. Materials

Poly(vinyl alcohol) (+99 % hydrolyzed, MW ≈ 72,000 g/mol), phosphate-buffered saline (PBS), Dulbecco's Modified Eagle Medium (DMEM), dimethyl sulfoxide (DMSO), bovine serum albumin (BSA) and 3-(4,5-dimethylthiazol-2-yl)-2,5-diphenyltetrazolium

bromide (MTT) were purchased from Sigma-Aldrich (St Louis, USA). Zinc oxide nanoparticles (+99 % purity, 35–45 nm) were obtained from US Research Nanomaterials (Houston, USA). Citric acid was supplied by Merck (Darmstadt, Germany). Ketamine and xylazine were purchased from Alfasan (Woerden, Netherlands). Deionized water was used for the preparation and characterization of mesh samples. All chemicals were of analytical reagent grade and used without further purification.

2.2. Fabrication of the hernia mesh samples

Four mesh samples were synthesized and examined in this study: PVA, PVA-ZnO, PVA-ZnO-PX, and PVA-ZnO-PX-CA. The fabrication procedure of each mesh is described as follows:

Preparation of the PVA film: A 10 % (w/w) aqueous solution of PVA was prepared by dissolving 4 g of PVA powder into 36 g of water for 4 h, using a magnetic hot plate stirrer (Heidolph, MR Hei-Standard) at 90 °C and 500 rpm. This solution was cast into a 10×10 cm^2 mold and cooled at room environment.

Preparation of the PVA-ZnO film: 0.02 g of ZnO NPs was added to the aforementioned PVA solution and stirred for 30 min at 90 °C and 500 rpm to make a homogenized solution. For the next 20 min, PVA-ZnO solution was placed into an ultrasonic bath (ACP-120H, MRC). Solution casting and cooling were then performed as mentioned above.

Preparation of the PVA-ZnO-PX film: After the PVA-ZnO film was obtained, physical crosslinking, including three repetitive freeze-thaw cycles, was applied. Each cycle was performed by placing the mold in a freezer (at −20 °C) and then room environment (at 24 °C) for 12 and 8 h, respectively.

Preparation of the PVA-ZnO-PX-CA film: After the previously-described PVA-ZnO solution was prepared, 0.2 g of CA, as a chemical crosslinker, was added and dissolved for 30 min at 90 °C and 500 rpm. The prepared solution was cast into the mold and cooled at room environment. Then, three cycles of freeze-thaw were performed according to the mentioned procedure.

As the final step, after the fabrication of PVA, PVA-ZnO, PVA-ZnO-PX and PVA-ZnO-PX-CA films, mesh pores were created by a self-made punch and die. The punch and die were made up of Mo40 steel alloy. The die possessed a length of 7 cm, a width of 5 cm and a height of 2 cm, as well as 99 holes. Each hole on the die had a diameter of 2 mm. Fig. 1a - d is a schematic of the preparation and placement of the desired PVA-based mesh graft.

2.3. Fourier-transform infrared spectroscopy

In order to analyze the chemical structure of samples, Fourier transform infrared spectroscopy (FT-IR) was employed using a Bruker Equinox 55 spectrometer (TENSOR 27, Germany). The attenuated total reflection (ATR) mode was used for FT-IR imaging, and the ATR crystal was zinc selenide (ZnSe). The scan range was between 4000 cm^{-1} and 600 cm^{-1}, and results were obtained with a spectral resolution of 4 cm^{-1}. A total number of 16 scans (4 scans for each sample) were taken.

2.4. Scanning electron microscopy analysis

A field emission scanning electron microscope (FESEM, Hitachi model S-4160, Japan) was utilized to visualize and investigate the surface morphology of PVA-ZnO mesh. The device was equipped with a field emission gun (FEG) as electron source and operated under 20 kV accelerating voltage. The working distance was set to 10 mm and the spatial resolution was 2 nm. SEM images were captured at 10,000x magnification. Prior to FESEM imaging, sample coating with gold (Au) was perfomed using a sputter coater (DSR1, Nano-Structured Coatings Co., Iran) to improve conductivity and reduce charging effects.

2.5. Swelling ratio

The swelling study was carried out based on the water uptake potential of prepared PVA-based samples. Meshes were cut into square pieces of 1×1 cm^2, completely dried in a vacuum oven at 50 °C for 24 h, and weighed (W_d). Then, samples were submerged in 20 mL of deionized water at 37 °C. After predetermined times (1, 4, and 24 h), samples were taken out, excess water on their surface was removed using filter papers, and weighed again (W_s). For each sample this experiment was repeated 3 times ($n = 3$). Swelling ratio values were determined according to the following equation:

$$\text{Swelling ratio}(\%) = \frac{W_s}{W_d} \times 100 \quad (1)$$

2.6. In vitro degradation

The biodegradation behavior of mesh grafts was evaluated through weight loss measurements during 42 days. After the initial weights of the samples (W_i) were determined, they were incubated (Binder CB150 CO_2 Incubator) in a sterile PBS solution at 37 °C and pH = 7.4. At specific time points (1, 14, 28, and 42 days), the specimens were removed, washed with deionized water, and fully vacuum dried. Finally, samples were weighed (W_f) and the weight loss percentage was calculated for each of them, as stated below:

$$\text{Weight loss}(\%) = \frac{W_i - W_f}{W_i} \times 100 \quad (2)$$

2.7. Water contact angle

Water contact angle (WCA) measurements were performed based on the sessile drop method, which involved dropping a 10 μL water droplet on the mesh surface and observing its deformation using a Krüss G10 contact angle measurement system (Germany). ImageJ software (drop analysis, LB-ADSA) was used to obtain contact angle values. For each sample, the test was repeated three times (n = 3) on average.

2.8. Mechanical properties

To evaluate the mechanical properties of the fabricated meshes, SANTAM universal tensile testing device (Iran, SPM20) was utilized. Samples were cut into rectangular pieces with a width of 10 mm, thickness of 0.1 mm, and effective length of 20 mm. Tensile testing was conducted with a speed of 5 mm/min at room environment conditions. Obtained stress-strain curves were then used to calculate mechanical parameters (in terms of maximum tensile strength, Young's modulus, and percent elongation at break).

Tensile strength and elongation at break were also determined for the abdominal wall tissue. The preparations were made according to the literature [28], with a few changes. Briefly, full-thickness 3×4 cm^2 specimens were recovered (under conditions thoroughly explained in *section* [29].). The composite specimens contained the entire repair site, including both the mesh (Prolene® or PVA-ZnO-PX-CA) and the associated abdominal wall tissue. The tests were carried out at a speed of 10 mm/min.

2.9. Cytotoxicity assay

In vitro cytotoxicity of the samples was assessed by determining the viability of L-929 fibroblast cells, using 3-(4,5-dimethylthiazol-2-yl)-2,5-diphenyltetrazolium bromide assay (MTT). Mouse fibroblast cells were obtained from the Pasteur Institute of Iran (Tehran, Iran), and the assay was conducted in accordance with [20], with slight changes.

Mesh samples were cut into pieces of 1×1 cm^2, and sterilized by UV light for 1 h. They were then completely dipped into PBS for 30min, and placed in a 96-well microplate. Fibroblast cells were cultured in Dulbecco's Modified Eagle Medium (DMEM) with 10 % PBS at a density of 2×10^4 cells.mL^{-1} and incubated for 24 h at 37 °C in a 5 % CO_2 incubator (Binder CB150 CO_2 Incubator). They were then seeded into the 96-well microplate. After 1, 3, and 7 days, 20 μL of MTT solution (1 mg mL^{-1} in medium without phenol red) was added to each plate well and incubated for 3 h in a humidified atmosphere. Finally, the solubilization solution (dimethyl sulfoxide, DMSO) was added to dissolve insoluble formazan crystals. The absorbance of the dissolved crystals was read at 570 nm wavelength. At each time point, cell viability percent was calculated according to the below equation:

$$\text{Cell viability}(\%) = \frac{OD_{sample}}{OD_{control}} \times 100 \quad (3)$$

where OD_{sample} and $OD_{control}$ are related to the cells treated with the desired mesh (PVA-ZnO-PX-CA) and cells with no treatment, respectively.

2.10. Surgical procedure

This investigation conformed to all animal ethics committee requirements (approval number: IR.TUMS.AEC.1401.080 provided by the Institutional Animal Care and Use Committee of the Tehran University of Medical Sciences). In this study, we used 16 adult male Sprague–Dawley rats aged 14–18 weeks (mean weight: 300 ± 20 g). All of them were kept under the standard situation with 22 ± 2 °C, 50 ± 20 % humidity, 12 h of light, and 12 h of darkness, free of any pathogen conditions as well. The rats were given free access to water and food during the whole study. They were divided into two groups of eight: Control with standard Prolene® mesh and experimental with PVA-ZnO-PX-CA mesh.

Animals were anesthetized using Ketamine/Xylazine (50/20 mg kg^{-1}) with intraperitoneal (IP) injection. Then, they were placed in the supine position with their extremities fixed on the operating table. Each animal's abdomen was shaved and prepared under anesthesia. All surgical operations were carried out in a sterile condition.

A 5 cm ventral midline skin incision starting 1 cm below the sternum was made. Then, in all rats, a full-thickness para-median abdominis muscle lesion was generated to a standard size of 2×3 cm^2. The fascial defect in the experimental group was repaired with PVA-ZnO-PX-CA and secured with a single interrupted 4-0 Prolene/silk stitch (Ethicon™, USA) at each of the four corners of the mesh and four extra sutures at the midway of the mesh.

In the control group, the defect was repaired using a Prolene® mesh (Ethicon™, USA), which was put over the defect, covering the incision by 5 mm circumferentially, and fixed with single interrupted 4-0 Prolene/silk sutures (Ethicon™, USA). The skin incisions were closed in a single interrupted way in all rats using 3-0 Vicryl (Ethicon™, USA). Animals were housed in separate cages after surgery and were observed regularly. Throughout the study, all animals were kept under the close care and underwent regular clinical examinations. Before or during the surgery, no antibiotic therapy was done.

All animals from each group were sacrificed 45 days after mesh implantation for morphological evaluations. The full-thickness abdominal wall specimen, including the graft and surrounding tissue, was removed and examined for tensile strength, histological examination, and adhesion formation. Photographs of the inner abdominal wall and the mesh location were obtained during the sacrifice. Fig. 2a - f represents the explained surgical procedure.

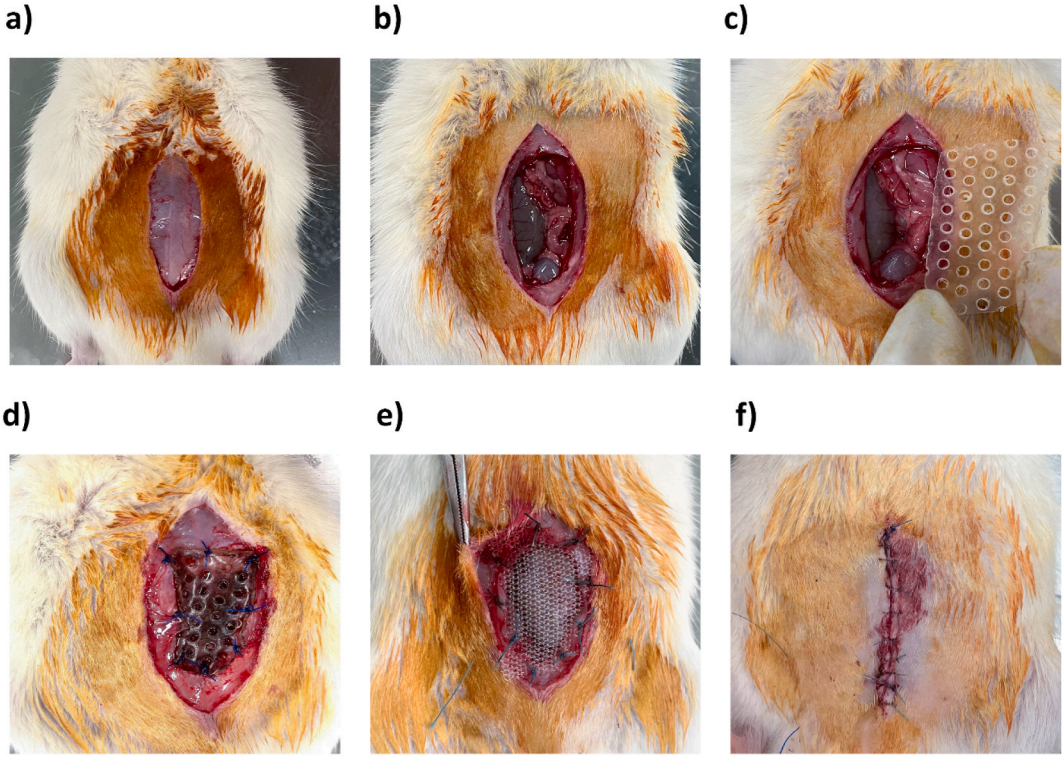

Fig. 2. Surgical procedure for *in vivo* studies: (a) creation of a ventral midline skin incision: the incision was 5 cm long and started from 1 cm below the sternum; (b) generation of a full-thickness para-median abdominis muscle lesion: the fascial defect had an approximate area of 2 × 3 cm^2; (c–d) placement and fixation of the PVA-ZnO-PX-CA mesh using eight single interrupted 4-0 Prolene/silk stitches; (e) implementation of the Prolene® mesh secured with nine single interrupted 4-0 Prolene/silk sutures; (f) stitching the skin incision in a single interrupted way using 3-0 Vicryl.

Table 1
Vandendael scoring [29] used for precise and reliable evaluation of local adhesion formation. This scoring system is based on four parameters: width (mm), thickness (mm), strength (subjective) and number of visible adhesion strands. Each parameter scores from 1 to 3. A total adhesion grade of 1–4 is considered as mild (grade I), 5–8 as moderate (grade II) and 9–12 as severe adhesion (grade III).

Parameter	Criteria	Scoring points
Width	<2 mm	1
	2–10 mm	2
	>10 mm	3
Thickness	<1 mm	1
	1–3 mm	2
	>3 mm	3
Strength	+	1
	++	2
	+++	3
Amount	0–2	1
	3–4	2
	>4	3

2.11. Adhesion formation

On day 45, post-operative adhesion formation was calculated qualitatively and semi-quantitatively according to the Vandendael score [29], by evaluating the mesh and underlying tissue. The method of scoring is presented in Table 1, and the total scoring points range from 4 to 12.

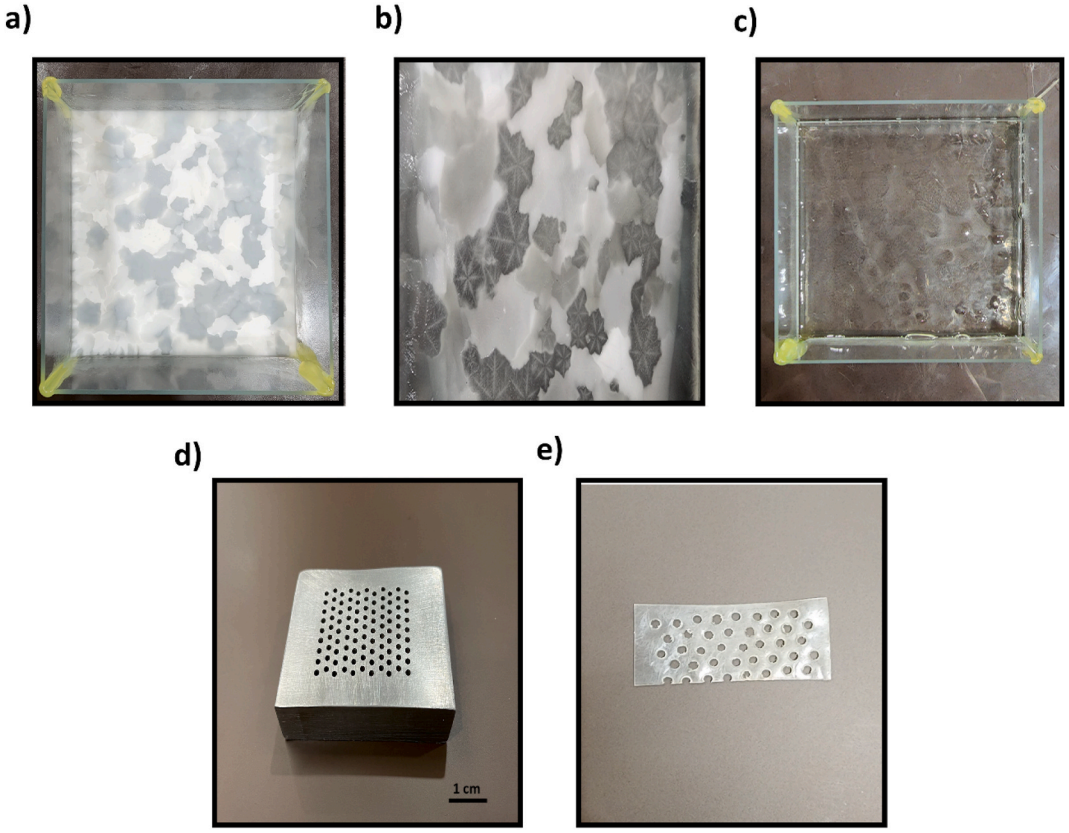

Fig. 3. (a–c) Resultant PVA-ZnO-CA film after 12 h at −20 °C (complete freezing), 6 h at −20 °C (clear formation of polycrystals of ice), and 8 h at 24 °C (complete thawing), respectively; (d) self-made die composed of Mo40 steel alloy having a volume of 7 (length) × 5 (width) × 2 (height) cm^3, as well as 99 holes; (e) final PVA-ZnO-PX-CA mesh after creation of mesh pores with a diameter of 2 mm. Each pore is spaced 2.5 mm apart from its neighboring pores.

2.12. Incorporation and shrinkage of the mesh

The mesh was lifted from the abdominal wall on all edges; a slide caliper was used to calculate incorporation to examine adhering tissue between the abdominal wall and the mesh, which was expressed as percentage. The remaining mesh's millimeter dimensions on each side were counted. The implanted mesh was typically 30 mm long and 20 mm wide. The mesh's sides were then measured to determine how many millimeters of each side showed incorporation.

By measuring the surface area of the mesh at the time of sacrifice, shrinkage of the mesh was measured. The mesh surface discovered during sacrifice was measured using a standardized caliper, then compared to the standardized implant size (6 cm^2), and expressed as a percentage of this standardized implant.

2.13. Abscesses

The abdominal cavity of all rats was assessed with visual inspection and examination on the last day of the study to evaluate the presence of abscesses or intra-abdominal infection.

2.14. Histological evaluation

The biocompatibility of each implanted mesh material was assessed using either trichrome blue staining or hematoxylin and eosin (H&E). All rats were sacrificed on day 45, and a full-thickness abdominal wall sample with an area of 2 × 0.5 cm^2 was harvested. This sample, which included both the abdominal wall and the mesh, was taken from one of the long sides. Samples were fixed in 4 % formalin, embedded in paraffin, sectioned (4 μm), mounted on microscope slides, and H&E stained right away. An experienced pathologist histologically evaluated all slides in a blind method [30]. Total multinucleate foreign body giant cells surrounding the mesh fiber, new blood vessels per visual field, the number of inflammatory cells, connective tissue formation, and collagen organization were assessed.

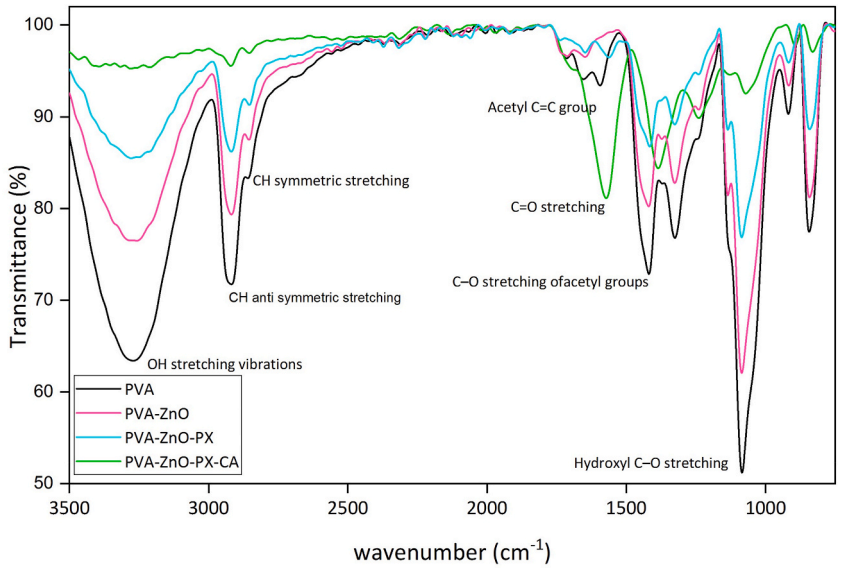

Fig. 4. ATR-FTIR spectra of PVA, PVA-ZnO, PVA-ZnO-PX and PVA-ZnO-PX-CA mesh samples. For each sample four scans were averaged. The scan range and spectral resolution were 4000-600 cm^{-1} and 4 cm^{-1}, respectively. *Note: PVA: poly(vinyl alcohol), ZnO: zinc oxide, PX: physical crosslinking, CA: citric acid.*

2.15. Histochemical analysis

Samples were fixed for 25 min at 4 °C in a solution of 4 % paraformaldehyde. The blocking procedure was performed with a 5 % gout serum (Gibco, USA; diluted in PBS buffer). The samples were incubated with fluorescein isothiocyanate–conjugated secondary antibodies (Abcam, UK; diluted in BSA/PBS, 0.2 %) for 1 h at 25 °C. In a high-power field, positively stained cells were counted. ImageJ software (NIH, USA) was used to evaluate and analyze results.

2.16. Statistical analysis

Statistical package for social sciences (SPSS) was used to conduct the statistical analysis. All results except for the mechanical characteristics of the dry meshes are presented as mean ± standard deviation (STD). The independent samples T-test was used and for *in vivo* evaluations and all data are presented by 95 % confidence interval; p values less than 0.05 were considered significant.

3. Results and discussion

3.1. Fabrication of the hernia mesh samples

Dissolving both ZnO and CA in PVA aqueous solution was performed at 90 °C and 500 rpm. Three cycles of freeze-thaw were carried out on the PVA-ZnO-CA solution. Fig. 3a and c shows the resultant PVA-ZnO-PX-CA sample after complete freezing and thawing of a cycle were achieved, respectively. Fig. 3b was obtained in the middle of the freezing process, after keeping the sample at −20 °C for 6 h. The formation of polycrystals of frozen solvent (ice) is clearly observed.

Mesh pores were cut using a self-made punch and die (Fig. 3d). Each pore had a diameter of 2 mm and was in an equal distance from adjacent pores (Fig. 3e). According to the classification presented by Earle and Mark [31], the synthesized meshes fit in the category of "large pore". Large pore diameters may lead to enhanced tissue-ingrowth, fibroplasia, and angiogenesis. However, a higher risk of adhesion and fistula formation can arise [32].

3.2. Fourier-transform infrared spectroscopy

FT-IR spectrums of pure PVA, PVA-ZnO, PVA-ZnO-PX, and PVA-ZnO-PX-CA samples are shown in Fig. 4. Measurements were performed at room temperature and the IR spectra wavenumber was adjusted from 4000 cm^{-1} to 600 cm^{-1}.

Characteristic vibration bands of PVA correspond to the peaks at 2930, 1413, 1332, 1090, and 920 cm^{-1}. The peak around 3295 cm^{-1} belongs to H–OH stretching. The presence of $–CH_2$ asymmetric and symmetric stretching is concluded from the peaks at 2930 and 2853 cm^{-1}, respectively. The band around 1413 cm^{-1} represents $–CH_3$ bending and the band around 1332 cm^{-1} is for $–CH_2$ stretching vibration. The peak at 1090 cm^{-1} corresponds to C–O stretching, resulting from the crystallinity of PVA. On the other hand, due to the syndiotactic structure of this polymer, $–CH_2$ rocking vibration is reported at 920 cm^{-1}. The existence of C═O band at 1719 cm^{-1} is

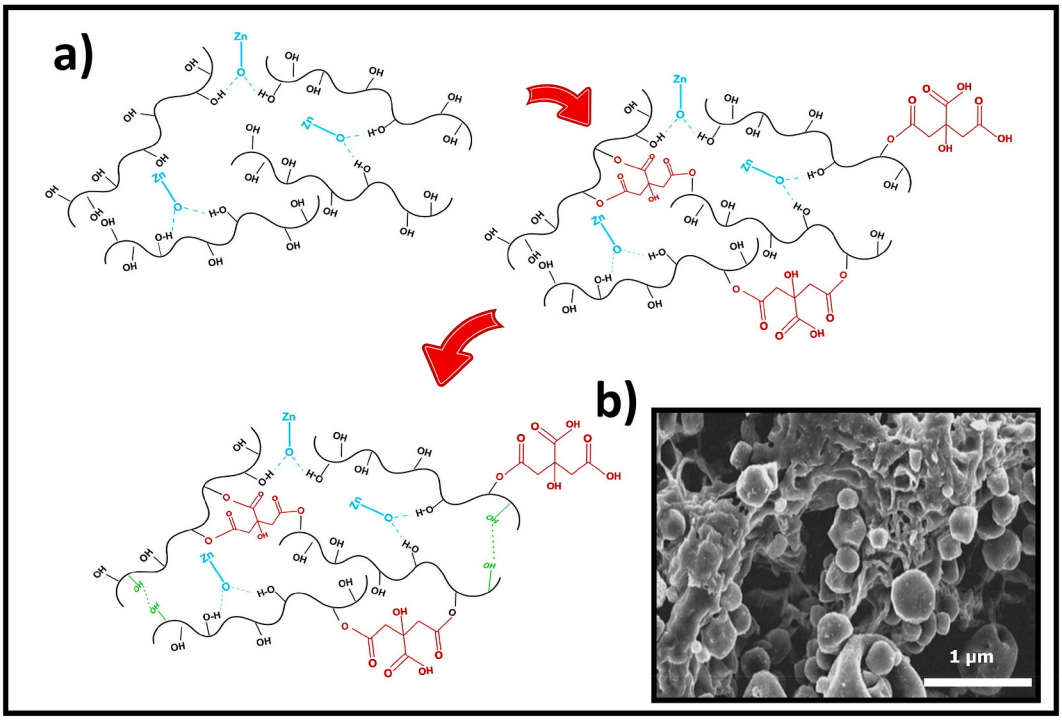

Fig. 5. (a) Effects of incorporating ZnO, CA and performing physical crosslinking, on the structure of PVA matrix in 2D dimensions. ZnO NPs form hydrogen bonds with the hydroxyl groups of PVA. Addition of CA leads to an esterification reaction between hydroxyl groups of PVA and carboxyl groups of CA, which is accompanied by releasing water. Freeze-thaw cycles can increase and strengthen the formation of hydrogen bonds between PVA chains. Solid and dotted lines represent chemical and physical bonds, respectively; (b) SEM image of PVA-ZnO sample magnified 10,000 times, showing the presence and proper dispersion of ZnO NPs.

because of the absorption of remaining acetate groups during poly(vinyl acetate) hydrolysis to form PVA. In addition, the peak at 839 cm^{-1} is for C–O stretching vibration. Our results are in agreement with those reported before [33–35].

As presented in Fig. 4, adding ZnO NPs and performing three cycles of freeze-thaw lead to marginal shifts in the wavenumber, while the intensity of the aforementioned peaks underwent a decrease. It should be noted that according to the literature [36], an absorption peak around 550-430 cm^{-1} was attributed to Zn–O stretching, in PVA-ZnO composites. However, this wavenumber fell outside of the scope of our spectrometer.

In the presence of citric acid, the new band found at 1600 cm^{-1} corresponds to C═O stretching vibration peak from ester groups. This peak indicates that the esterification reaction occurred between carboxyl groups of CA and hydroxyl groups of PVA [37]. Moreover, its height can reflect the degree of esterification [38].

3.3. Scanning electron microscopy analysis

Fig. 5a illustrates the formation of new bonds in the PVA matrix when different modifications were applied. The incorporation of ZnO NPs resulted in the formation of hydrogen bonds with hydroxyl groups of PVA. Adding CA created ester bonds, due to the chemical reaction between CA carboxyl groups and PVA hydroxyl groups. Furthermore, the freeze-thaw process is based on the existence of regular pendant OH groups on PVA, being able to form crystallites by strong inter-chain hydrogen bonding [39]. Thus, it can be inferred that the three chemical/physical modifications alter PVA constitution and structure through affecting OH functional groups.

The surface morphological structure of PVA-ZnO was investigated using FESEM analysis, with a magnification of 10,000x. Fig. 5b presents a scanning electron micrograph of the fabricated PVA-ZnO sample, where the presence and relatively uniform dispersion of ZnO NPs can be perceived.

3.4. Swelling ratio

The water uptake capacity is a key indication of biocompatibility and applicability for biomedical purposes [40]. The swelling percent of PVA, PVA-ZnO, and crosslinked PVA-ZnO specimens were calculated using Equation (1), and the results are illustrated in Fig. 6a. Hydrophilic groups enhance water absorption and swelling properties. Thus, PVA polymer benefits from having a large hydroxyl number, forming hydrogen bonds with water. However, the addition of ZnO NPs can involve some of the active OHs, which results in a decrease in swelling capacity [26,41]. Similarly, with the inclusion of CA as a chemical crosslinking agent, a number of PVA

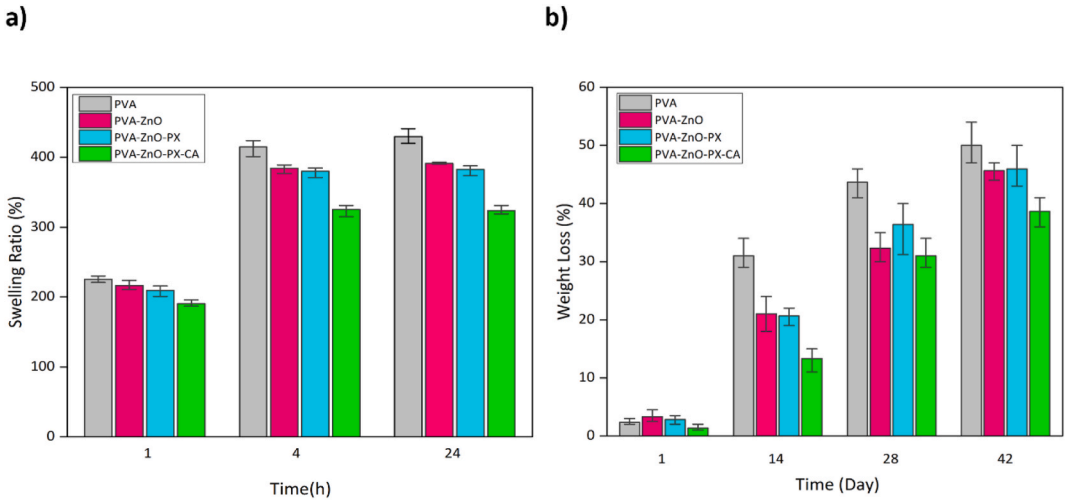

Fig. 6. (a) Swelling percentages of PVA, PVA-ZnO, PVA-ZnO-PX, and PVA-ZnO-PX-CA meshes measured after 1, 4, and 24 h of soaking in water, which indicates their water uptake capacity and potential biocompatibility (n = 3); (b) stability and biodegradation assessment of PVA, PVA-ZnO, PVA-ZnO-PX, and PVA-ZnO-PX-CA samples expressed as weight loss percentages measured after 1, 14, 28, and 42 days of soaking in PBS solution (n = 3). *Note: PVA: poly(vinyl alcohol), ZnO: zinc oxide, PX: physical crosslinking, CA: citric acid.*

polar groups participate in an esterification reaction, leading to a decrement in swelling degree [38]. Furthermore, three freeze-thaw cycles form a physically crosslinked network that increases crystallinity and intermolecular forces among polymer chains. These would decrease PVA chains mobility and vacancies for the accommodation of water molecules, thereby lessening water absorption [40].

As explained above, the swelling ratio comparison of the designed samples in all three time intervals can be expressed as follow: PVA > PVA-ZnO > PVA-ZnO-PX > PVA-ZnO-PX-CA. Significant difference in the swelling ratio of PVA-ZnO sample can be perceived in comparison with pure PVA and PVA-ZnO-PX-CA meshes, after 4 and 24 h of soaking. Moreover, physical crosslinking had minimal effects on the swelling capacity of PVA-ZnO mesh. Results also indicate that swelling equilibrium was achieved after 24 h of immersion in water.

3.5. *In vitro degradation*

The major complication of absorbable/degradable meshes relates to their high degradation rate. Therefore, a bioabsorbable mesh should be tailored in a way that its degradation rate matches the required time for tissue in-growth, thereby preventing hernia recurrence [42].

The stability of mesh samples was assessed by weight loss measurements at four time points (1, 14, 28, and 42 days), using Equation (2). Obtained results are presented in Fig. 6b. It can be observed that the weight loss of all samples increased with immersion time. From day 1–14, pure PVA mesh degraded at a faster rate and reached 30 ± 3 %. After this period, the sample lost weight in a slower manner and reached up to 49 ± 4.5 %, at the end of 42 days.

Involving ZnO content decreased the biodegradation rates to 21 ± 4.5 % and 32 ± 3.2 % on days 14 and 28, respectively. Barua et al. [43] reported that excessive addition of ZnO NPs would lead to a decline in biodegradability of Hydroxyapatite/Poly(methyl methacrylate)/ZnO composite bone scaffold. Our results are also in agreement with Feng et al.' study [44] on the fabrication of a β-tricalcium phosphate/ZnO scaffold for bone tissue engineering. Furthermore, the application of freeze-thaw cycles generally delays weight loss percent in PBS solution [45]. However, in this work, physical crosslinking had a marginal effect on the biodegradability of the PVA-ZnO sample, similar to what was observed in *section 3.4* **Swelling ratio**.

When CA was added, the stability of the mesh was noticeably enhanced to 14 ± 3.2 %, 30 ± 3 %, and 39 ± 3.5 %, after 14, 28, and 42 days of incubation in PBS. This result is consistent with the literature [46,47]. The reasons behind how ZnO NPs and crosslinking techniques affect *in vitro* degradation are comparable to the explanation given in *section 3.4* **Swelling ratio**: The formation of a more crystalline structure, as well as the involvement of PVA polar groups, would allow less fluid into the polymer matrix, thereby diminishing the weight loss percentage.

3.6. *Water contact angle*

The wetting behavior of neat PVA, PVA-ZnO, PVA-ZnO-PX, and PVA-ZnO-PX-CA grafts was investigated by determining water contact angle (WCA) values, as shown in Fig. 7a, b. The measurements were based on the deformation of the water droplet, 60 s after it was dropped on the surface of the samples.

Each modification applied to the neat PVA mesh resulted in an increase in contact angle degree. Greater values of contact angle mean less tendency to water absorption, thus higher surface hydrophobicity. The role of ZnO NPs and freeze-thaw cycles on the

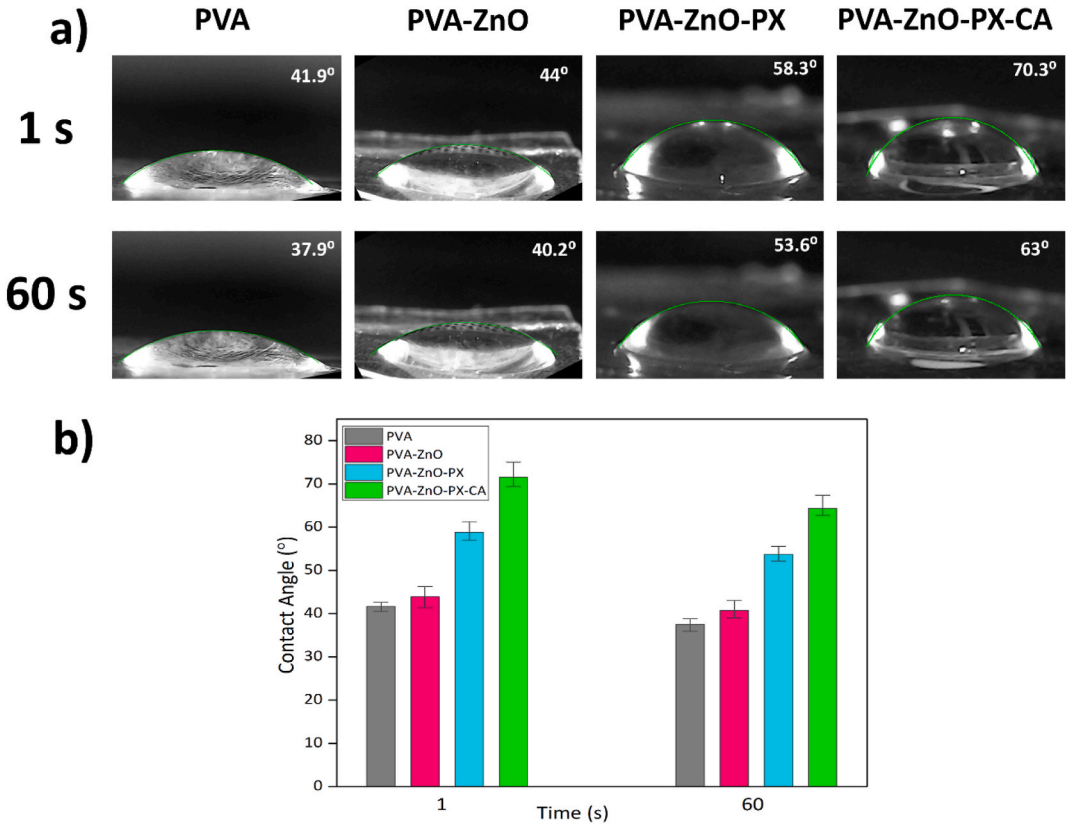

Fig. 7. Water contact angle measurements of PVA, PVA-ZnO, PVA-ZnO-PXA and PVA-ZnO-PX-CA based on the sessile drop method immediately and 60 s after the water droplet was dropped on the mesh surface: (a) results analyzed by ImageJ; (b) results presented in bar diagram. Contact angle values below 90° represent hydrophilic samples. *Note: PVA: poly(vinyl alcohol), ZnO: zinc oxide, PX: physical crosslinking, CA: citric acid.*

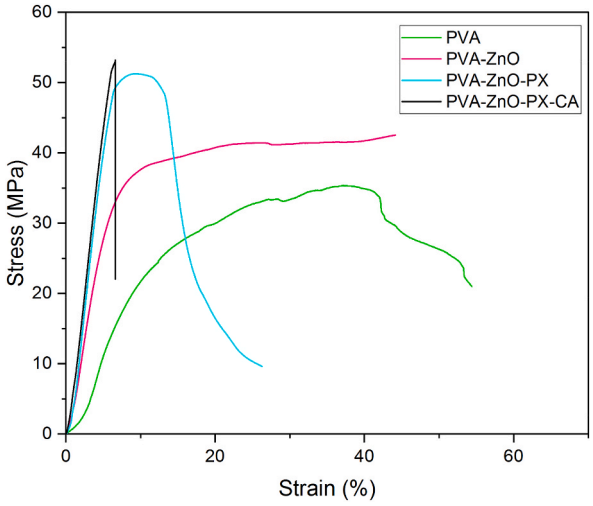

Fig. 8. Stress-strain diagrams of PVA, PVA-ZnO, PVA-ZnO-PX and PVA-ZnO-PX-CA specimens, used to assess their mechanical properties in terms of maximum tensile strength, Young's modulus and %elongation at break (n = 3). *Note: PVA: poly(vinyl alcohol), ZnO: zinc oxide, PX: physical cross-linking, CA: citric acid.*

elevation of the WCA value is due to forming a more compact structure. Furthermore, the presence of these NPs on the surface of the mesh facilitates air adsorption, thereby hindering the penetration of water molecules [48–50]. Finally, crosslinking with CA decreases the capacity of water absorbency, based on two reasons: I) formation of ester bonds, II) reduced molecular interactions between the

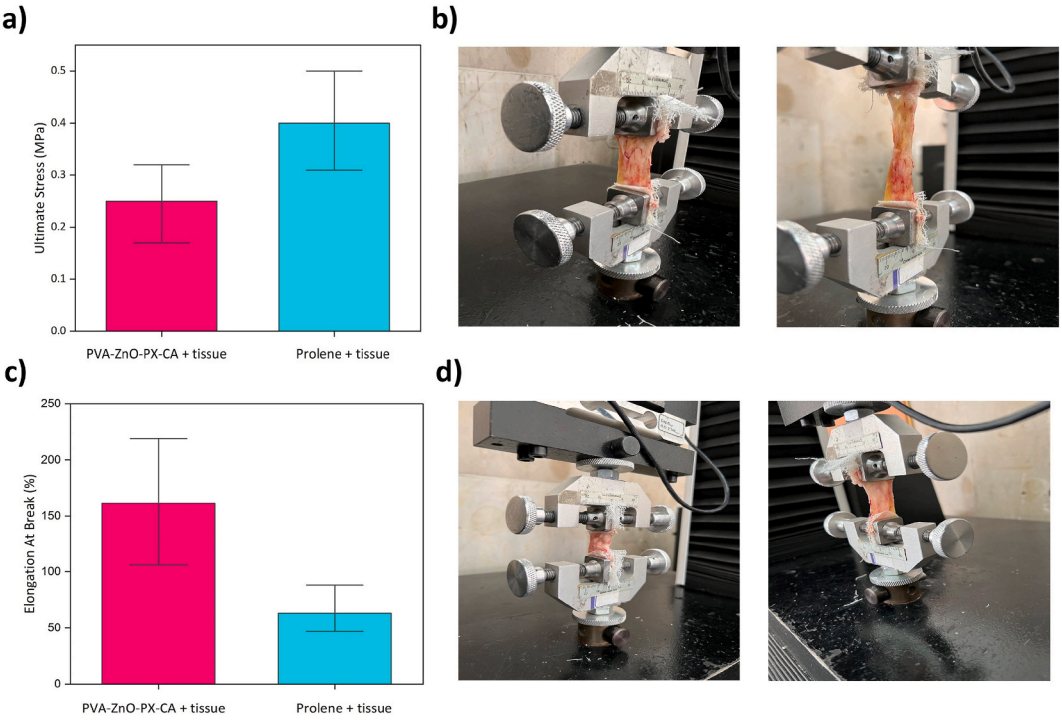

Fig. 9. Performing tensile tests for the Prolene®+abdominal wall tissue (control) and PVA-ZnO-PX-CA + abdominal wall tissue (experimental) specimens, and comparing their mechanical properties (n = 3). These specimens were obtained after rats were sacrificed on day 45 postoperative: (a) maximum tensile strength of Prolene®+tissue and PVA-ZnO-PX-CA + tissue; (b) tensile testing of the experimental group performed at the speed of 10 mm/min; (c) elongation at break (%) of Prolene®+tissue and PVA-ZnO-PX-CA + tissue; (d) tensile testing of the control group performed at the speed of 10 mm/min. *Note: PVA: poly(vinyl alcohol), ZnO: zinc oxide, PX: physical crosslinking, CA: citric acid.*

water droplet and the surface of the samples [37].

Therefore, PVA and PVA-ZnO-PX-CA obtain the highest and lowest affinity for water, respectively. Compared to neat PVA, water contact angles of PVA-ZnO, PVA-ZnO-PX, and PVA-ZnO-PX-CA are increased by 6.07, 41.42, and 66.23 %, respectively. It should be mentioned that all of the reported values are less than 90°, indicating that our samples are still highly hydrophilic, mainly due to the existence of plenty of hydroxyl groups in the backbone of the PVA mesh [50].

3.7. Mechanical properties

The mechanical properties of the specimens were evaluated in terms of ultimate tensile strength, elongation at break, and Young's (elastic) modulus. Fig. 8 represents the obtained stress-strain curves based on the dry state.

According to the results, the tensile strength of the PVA mesh with no ZnO content is 35.2 ± 1.1 MPa. However, incorporating ZnO NPs and using freeze-thaw cycles enhance this property to 42.2 ± 2.1 and 52.3 ± 1.7 MPa, respectively. The highest strength is achieved at 52.8 ± 2.3 MPa when both crosslinking methods are applied. Research group of Idrees [32] reported that for hernias of large size, the burst pressure and tensile strength of the surgical meshes should be at least 180 mmHg and 32 N/cm, respectively. Thus, all of these four samples possess acceptable tensile strength values. Regarding Young's modulus, samples follow the same order as ultimate strength, with neat PVA and PVA-ZnO-PX-CA obtaining the lowest (222 ± 7.6 MPa) and greatest (780 ± 23.6) elastic modulus values, respectively.

Imaan et al. [51] fabricated PVA-ZnO composite membranes with different ZnO contents. They stated that an increase in the incorporated ZnO level enhances the strength of the composite due to dispersion, high surface area, and intermolecular interactions of ZnO with PVA. In addition, freeze-thawing helps the mesh structure become more compact by creating crystallites and secondary bonds [40]. Similarly, utilizing low amounts of CA as a chemical crosslinker strengthened the network structure, followed by greater resistance to lengthwise stress and stiffness. It should be mentioned that as the concentration of CA grows, it can act as a plasticizer as well, which has opposite effects on mechanical properties [38].

Fig. 8 also implies that using ZnO NPs, three cycles of freeze-thaw and CA crosslinking agent decreased elongation at break values and improved brittleness of the designed meshes. Percentage elongation of PVA, PVA-ZnO, PVA-ZnO-PX, and PVA-ZnO-PX-CA specimens can be respectively described as 54.4 ± 2.8, 44 ± 1.9, 25.8 ± 0.9, and 6.7 ± 0.4 %.

Besides dry mesh grafts, tensile tests were also conducted for the mesh + tissue samples. Fig. 9a - d illustrates the ultimate strength and percentage elongation of PVA-ZnO-PX-CA + tissue (case) and Prolene®+tissue (control) specimens. These specimens include both

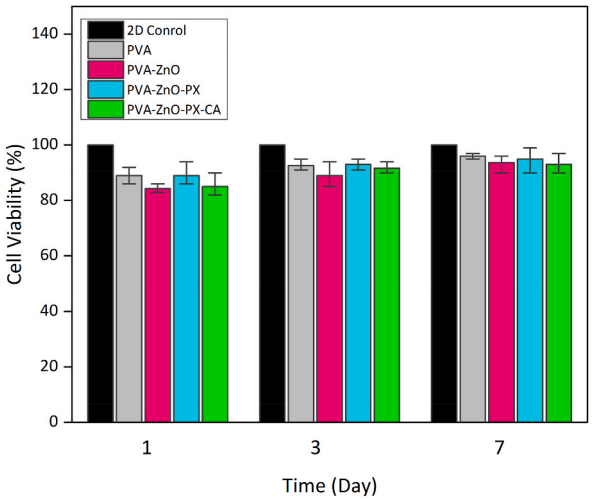

Fig. 10. Cell viability calculation of PVA, PVA-ZnO, PVA-ZnO-PX and PVA-ZnO-PX-CA samples based on 100 % viability of cells in 2D control group at each time interval. MTT assay was performed for the cytotoxicity evaluation and results were achieved 1, 3 and 7 days after cell culture. *Note: 2D control: 2D cell culture, PVA: poly(vinyl alcohol), ZnO: zinc oxide, PX: physical crosslinking, CA: citric acid.*

implanted mesh and associated abdominal wall tissue.

It can be perceived that the proposed modified mesh acquired lower tensile strength values (case: 0.24 ± 0.07 MPa, control: 0.4 ± 0.1 MPa), and higher elongation% (case: 162.5 ± 50 %, control: 65 ± 18 %). These results were expected since Prolene® is a non-absorbable/non-degradable polymer.

3.8. Cytotoxicity assay

The potential cytotoxicity of the designed meshes was evaluated by MTT assay. L-929 fibroblast cells were utilized in this test since fibroblasts are the main cells that cover the surface of the mesh in the early and late phases of wound healing, and play an important role in collagen formation on the mesh surface. Cell viability (%) was determined on days 1, 3, and 7, regarding Equation (3). At each time point, the viability of cells in contact with mesh samples was calculated based on 100 % viable cells from the control group.

Fig. 10 indicates that the cell viability of all pure and modified PVA samples was higher than 80 %. Therefore, the examined meshes exhibit no cytotoxic effect on the fibroblast cells. When modifications were applied to the PVA mesh, slight changes can be seen in the number of viable cells. However, no significant difference exists between any two groups treated with different PVA-based meshes.

3.9. Surgical procedure

All 16 rats survived the operation and thrived until necropsy at the end of the trial. There was no evidence of recurring hernias in any of the rats at necropsy. Furthermore, no evidence of infection was found during the trial. There were no variations in weight gain or loss between the two groups.

3.10. Adhesion formation

All animals showed some signs of visceral adhesion development 45 days after implantation. Fig. 11 displays representative macroscopic images of the experimental (Fig. 11a) and control group (Fig. 11b). Calculating the adhesion score according to the Vandendael scoring [29], the PVA-ZnO-PX-CA mesh showed lower values (median = 6.7, range: 4–9) than the Prolene® mesh (median = 9, range: 5–12) (Fig. 11c).

Intra-abdominal adhesion formation is an important complication following herniorrhaphy with mesh placement surgery [52]. An adhesion band may connect visceral organs to the mesh surface, which complicates the procedure of intra-abdominal hernia repair. This complication can potentially lead to bowel erosion, obstruction, and fistula formation [53].

Prolene®, as the standard intra-abdominal mesh, showed the most adhesions (54.1 %) compared to other surgical mesh grafts [54]. According to the results of this study, our assumption is that the proposed mesh based on PVA shows less tendency to develop adhesions in addition to providing appropriate support for the abdominal wall. We presume that the non-adhesiveness of this synthetic mesh was enhanced due to obtaining a more hydrophobic characteristic, as concluded from the swelling ratio and water contact angle measurements. As reported by Li et al. [55], improving hydrophobicity to some extent, can lead to a better anti-adhesion effect.

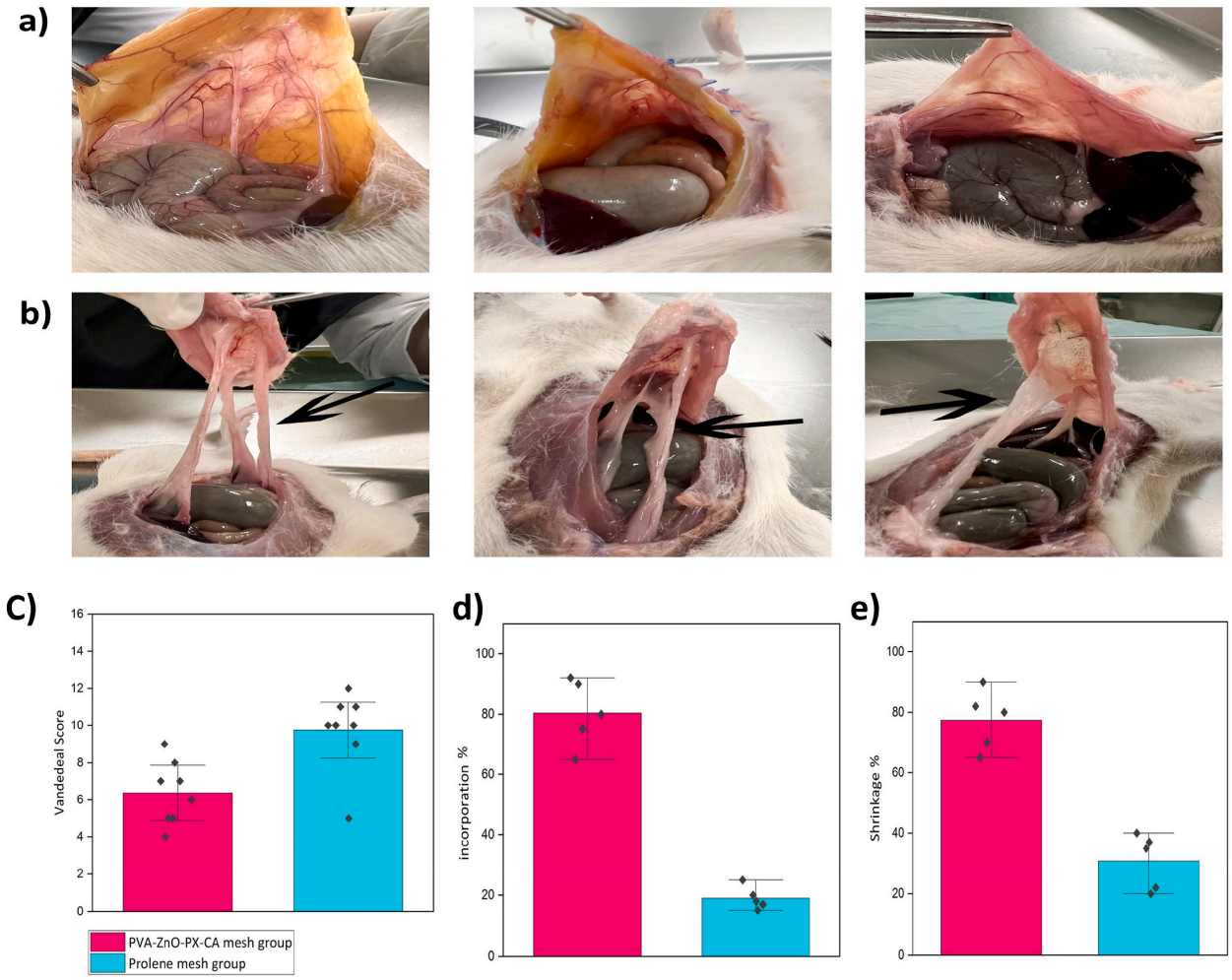

Fig. 11. (a–b) Macroscopic images of the repaired herniated sites and visceral adhesion formation on day 45 post-operative in the experimental (treated with PVA-ZnO-PX-CA mesh) and control (treated with Prolene® mesh) group, respectively. Thick adhesions can be noticed in the control group (shown with black arrows); (c) calculation of adhesion formation based on the Vandendael scoring method [29]; (d) tissue integration of the proposed PVA-ZnO-PX-CA and conventional Prolene® mesh patches; (e) shrinkage of the PVA-ZnO-PX-CA vs. Prolene® hernia mesh. *Note: PVA: poly (vinyl alcohol), ZnO: zinc oxide, PX: physical crosslinking, CA: citric acid.*

3.11. Incorporation and shrinkage of the mesh

In this study, we report mesh incorporation as the proportion of the original surface area that was incorporated in tissue within 45 days after mesh implementation. It was observed that the intervention group which received PVA-ZnO-PX-CA mesh showed significantly greater incorporation in comparison to the control (79 ± 9 % vs. 21 ± 7 % respectively) (Fig. 11d). Similarly, the fabricated mesh showed greater shrinkage compared to the Prolene® mesh (76.2 ± 7.9 % vs. 20.6 ± 4.1 %) ($p < 0.001$) (Fig. 11e).

The results from the evaluation of incorporation and shrinkage demonstrate that PVA-ZnO-PX-CA performed superiorly in comparison with the conventional Prolene® mesh, which results in minor critical overlaps that might be due to lower fibrous tissue formation. This, in turn, minimizes the rate of hernia recurrence at the mesh borders and dislocation of the prosthesis [56].

3.12. Abscesses

No abscesses were found on either of the meshes or in the intra-abdominal cavity in any of the rats of each group.

3.13. Histological evaluation

At both low and high magnification, 45 days after implantation, differences between the control and the PVA-ZnO-PX-CA mesh were noticeable in H&E slide show samples, as presented in Fig. 12a. When viewed at low magnification, the rectus muscles seemed

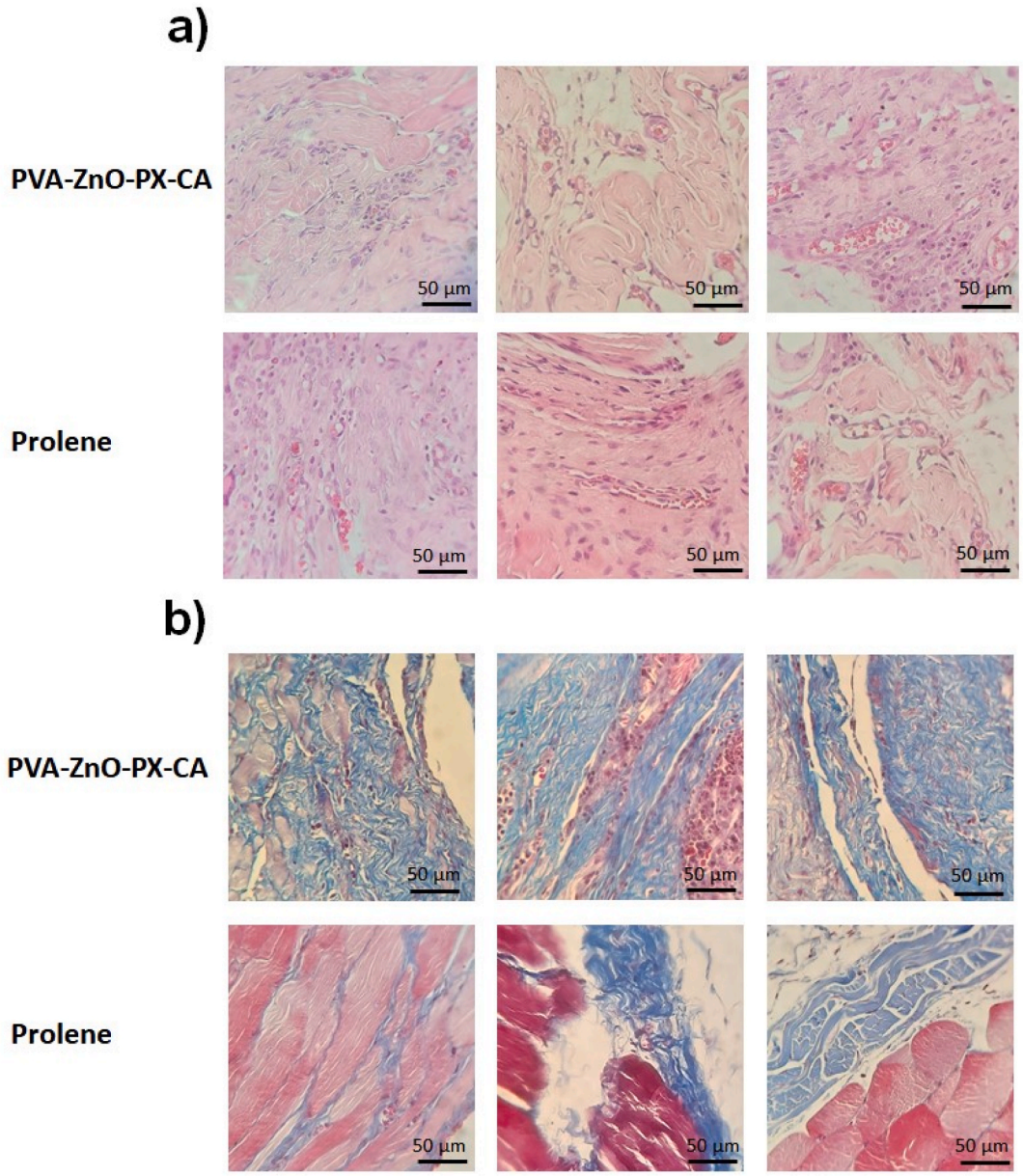

Fig. 12. Staining of the repaired abdominal wall tissue using PVA-ZnO-PX-CA mesh (case) and Prolene® mesh (control). The magnifications of all images are 400x: (a) H&E staining showing collagen deposition in the connective tissue, as well as more microvessel formation in the case group compared to the control group; (b) Masson's Trichrome staining indicating higher, thicker and denser collagen formation in the case group compared to the control group. *Note: PVA: poly(vinyl alcohol), ZnO: zinc oxide, PX: physical crosslinking, CA: citric acid.*

thinner in the control than the experimental group.

The samples' H&E staining revealed no noticeable difference between the two groups in the overall number of inflammatory cells, eosinophils, macrophages, or mononuclear cells. Extracellular matrix (ECM) deposition was minimal in all samples and did not significantly differ from the control sample.

Regarding the foreign body granuloma formation, it was observed that fewer granulomas were formed around the prepared mesh at the mesh-host tissue interface, compared to the Prolene® one. We surmise that even though we did not observe any inflammation-related cells 45 days post-operatively, the fewer granulomas might be an indication of higher biocompatibility and lesser immunologic reaction. On the other hand, Prolene® mesh is not biodegradable, whereas PVA is. This might help with preventing persistent inflammation and fibrous encapsulation.

The high power field study was utilized to measure the average number of neo-microvessels; this study shows that neovascularization has a substantially higher rate with PVA-ZnO-PX-CA, compared to Prolene® mesh (26.6 ± 1.3 vs. 11.7 ± 3.1) ($p <$

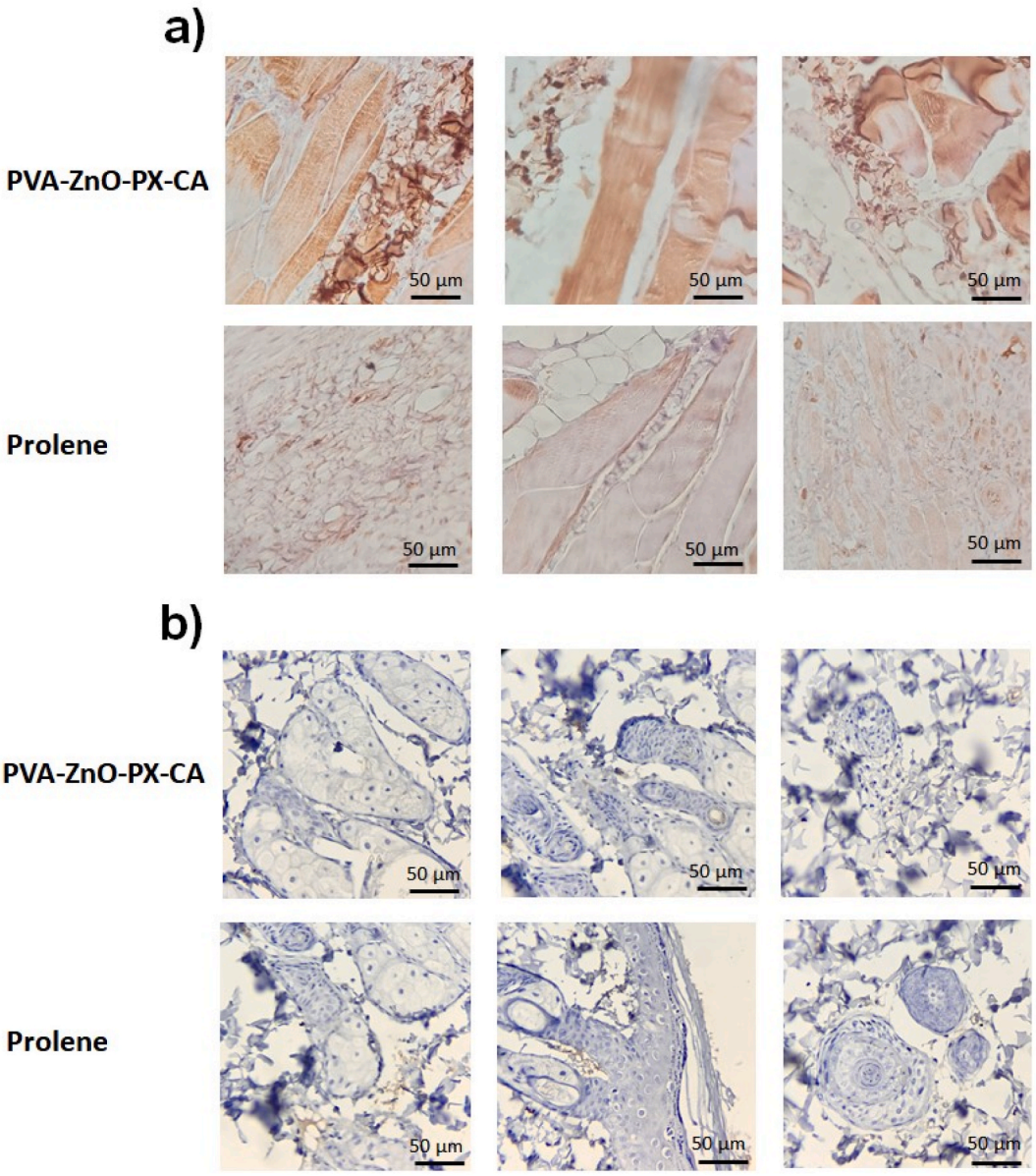

Fig. 13. Staining of the repaired abdominal wall tissue using PVA-ZnO-PX-CA mesh (case) and Prolene® mesh (control). The magnifications of all images are 400x: Significant increase in the levels of (a) PDGF and (b) TGF-β can be noted in the PVA-ZnO-PX-CA group compared to the Prolene® group according to the IHC staining. *Note: PVA: poly(vinyl alcohol), ZnO: zinc oxide, PX: physical crosslinking, CA: citric acid.*

0.05), which is indicative of the higher mesh incorporation.

3.14. Histochemical analysis

Collagen formation is essential for any repair. To measure collagen deposition, slices of the healed tissues were then stained using Masson's Trichrome (MT) staining. The amount of collagen formed in the experimental group was significantly higher than in the control group. Collagen fiber deposition was thick, regular, and dense in the cases treated with PVA-ZnO-PX-CA mesh. Collagen levels were lower in the control group, and the bundles were randomly distributed throughout the sample and weakly attached (Fig. 12b).

A growth factor that controls cell development and division is the platelet-derived growth factor (PDGF). In particular, PDGF is important for the development of blood vessels, the proliferation of mesenchymal cells, including fibroblasts and vascular smooth muscle cells, as well as cell-directed migration known as chemotaxis [57]. Thus, samples from the experimental and control groups were additionally stained with IHC to detect PDGF. The pictures of the IHC-stained samples (Fig. 13a) were analyzed with ImageJ. Results analysis revealed a significant (p value = 0.04) increase in the stained areas of samples treated with the PVA-ZnO-PX-CA mesh

(62 ± 5.9 %) compared with those treated with the conventional Prolene® (54 ± 3.3 %). This might explain better new blood vessel formation.

Transforming growth factor (TGF-β), a cytokine with a wide range of pleiotropic effects, is known to play a role in wound healing, angiogenesis, and immune modulation. TGF-β stimulates and regulates angiogenesis, a crucial component of healing. The fibrosis formation is known to be triggered by TGF-β, which is also known to cause excessive ECM synthesis and inhibit ECM degradation [58]. Therefore, we stained the tissues with immunohistochemistry (IHC) to measure the levels of TGF-β, as shown in Fig. 13b. The analysis of the TGF-β stained areas demonstrated that the stained area in the case and control groups were 86 ± 9.5 % and 70 ± 7.4 %, respectively ($p < 0.05$).

4. Conclusion

In conclusion, we fabricated an anti-adhesive mesh based on PVA, which underwent three freeze-thawing cycles for hernia repair. The results revealed that incorporation of ZnO NPs into the PVA matrix and further introduction of citric acid for chemical cross-linking, resulted in mechanical strength enhancement up to 52.8 ± 2.3 MPa. Moreover, freeze-thawing cycles induced the crystalline structures to contribute to mechanical reinforcement. Additionally, degradability analysis illustrated 39 ± 3.5 % weight loss for PVA-ZnO-PX-CA sample after 42 days, indicating an improvement in the resistance from degradation. These achievements may decrease hernia recurrence rates when absorbable meshes are used instead of permanent ones. *In vivo* studies also represented lower formation of local adhesions, higher formation of new vessels and enhanced levels of collagen deposition, PDGF and TGF-β factors. All the results indicate a notable potential of our fabricated mesh in hernia repair.

Funding

This research did not receive any specific grant from funding agencies in the public, commercial, or not-for-profit sectors.

Data availability

All data included in this study are available upon request by contact with the corresponding author (email address: smahmadit@sina.tums.ac.ir).

CRediT authorship contribution statement

Erfan Dorkhani: Writing – review & editing, Visualization, Validation, Resources, Project administration, Methodology, Investigation, Formal analysis, Data curation, Conceptualization. **Bahareh Darzi:** Writing – review & editing, Writing – original draft, Visualization, Validation, Investigation, Formal analysis, Data curation, Conceptualization. **Laleh Foroutani:** Writing – original draft, Visualization, Formal analysis, Data curation. **Zahra Ebrahim Soltani:** Formal analysis, Data curation. **Seyed Mohsen Ahmadi Tafti:** Writing – review & editing, Validation, Supervision, Resources, Methodology, Conceptualization.

Declaration of competing interest

The authors declare that they have no known competing financial interests or personal relationships that could have appeared to influence the work reported in this paper.

References

[1] G. Pascual, S. Sotomayor, M. Rodríguez, Y. Bayon, J.M. Bellón, Behaviour of a new composite mesh for the repair of full-thickness abdominal wall defects in a rabbit model, PLoS One 8 (11) (2013), e80647.
[2] K. Baylón, P. Rodríguez-Camarillo, A. Elías-Zúñiga, J.A. Díaz-Elizondo, R. Gilkerson, K. Lozano, Past, present and future of surgical meshes: a review, Membranes 7 (3) (2017) 47.
[3] A. Birindelli, M. Sartelli, S. Di Saverio, F. Coccolini, L. Ansaloni, G.H. van Ramshorst, G. Campanelli, V. Khokha, E.E. Moore, A. Peitzman, 2017 update of the WSES guidelines for emergency repair of complicated abdominal wall hernias, World J. Emerg. Surg. 12 (1) (2017) 1–16.
[4] C.W. See, T. Kim, D. Zhu, Hernia mesh and hernia repair: a review, Engin. Regener. 1 (2020) 19–33.
[5] J.W. Burger, R.W. Luijendijk, W.C. Hop, J.A. Halm, E.G. Verdaasdonk, J. Jeekel, Long-term follow-up of a randomized controlled trial of suture versus mesh repair of incisional hernia, Annals of surgery 240 (4) (2004) 578.
[6] M. Burati, A. Scaini, L.A. Fumagalli, F. Gabrielli, M. Chiarelli, Mesh fixation methods in Groin hernia surgery, in: A. Guttadauro (Ed.), Techniques and Innovation in Hernia Surgery, IntechOpen, 2019, pp. 99–107.
[7] A.S. Pandit, J.A. Henry, Design of surgical meshes–an engineering perspective, Technol. Health Care 12 (1) (2004) 51–65.
[8] G. Pascual, C. Mesa-Ciller, M. Rodríguez, B. Pérez-Köhler, V. Gómez-Gil, M. Fernández-Gutiérrez, J. San Román, J.M. Bellón, Pre-clinical assay of the tissue integration and mechanical adhesion of several types of cyanoacrylate adhesives in the fixation of lightweight polypropylene meshes for abdominal hernia repair, PLoS One 13 (11) (2018), e0206515.
[9] S. Kalaba, E. Gerhard, J.S. Winder, E.M. Pauli, R.S. Haluck, J. Yang, Design strategies and applications of biomaterials and devices for hernia repair, Bioact. Mater. 1 (1) (2016) 2–17.
[10] F. Corduas, D.A. Lamprou, E. Mancuso, Next-generation surgical meshes for drug delivery and tissue engineering applications: materials, design and emerging manufacturing technologies, Bio-Design and Manufacturing 4 (2) (2021) 278–310.
[11] D.I. Watson, S.K. Thompson, P.G. Devitt, L. Smith, S.D. Woods, A. Aly, S. Gan, P.A. Game, G.G. Jamieson, Laparoscopic repair of very large hiatus hernia with sutures versus absorbable mesh versus nonabsorbable mesh: a randomized controlled trial, Ann. Surg. 261 (2) (2015) 282–289.

[12] D.I. Watson, S.K. Thompson, P.G. Devitt, A. Aly, T. Irvine, S.D. Woods, S. Gan, P.A. Game, G.G. Jamieson, Five year follow-up of a randomized controlled trial of laparoscopic repair of very large hiatus hernia with sutures versus absorbable versus nonabsorbable mesh, Ann. Surg. 272 (2) (2020) 241–247.
[13] D.L. Sanders, A.N. Kingsnorth, Prosthetic mesh materials used in hernia surgery, Expet Rev. Med. Dev. 9 (2) (2012) 159–179.
[14] D. Fehér, A. Ferencz, G. Szabó, K. Juhos, D. Csukás, C. Voniatis, L. Reininger, K. Molnár, A. Jedlovszky-Hajdú, G. Wéber, Early and late effects of absorbable poly (vinyl alcohol) hernia mesh to tissue reconstruction, IET Nanobiotechnol. 15 (6) (2021) 565–574.
[15] K. Molnár, C. Voniatis, D. Feher, A. Ferencz, L. Fónyad, L. Reiniger, M. Zrínyi, G. Wéber, A. Jedlovszky-Hajdú, Biocompatibility study of poly (vinyl alcohol)-based electrospun scaffold for hernia repair, Express Polym. Lett. 12 (8) (2018) 676–687.
[16] D. Fehér, A. Ferencz, G. Szabó, L. Fónyad, K. Juhos, P.M. Guba, D. Csukás, J. Sándor, F. Ender, K. Molnár, A. Jedlovszky-Hajdú, M. Zrínyi, G. Wéber, Tissue engineered nanofiber poly (vinyl alcohol) mesh for the treatment of abdominal wall hernia, Int. J. Bio Technol. Res. 6 (2) (2016) 7–14.
[17] C. Voniatis, L. Balsevicius, D. Barczikai, D. Juriga, A. Takács, L. Kőhidai, K. Nagy, A. Jedlovszky-Hajdu, Co-electrospun polysuccinimide/poly (vinyl alcohol) composite meshes for tissue engineering, J. Mol. Liq. 306 (2020), 112895.
[18] C.S. Shin, F.J. Cabrera, R. Lee, J. Kim, R. Ammassam Veettil, M. Zaheer, A. Adumbumkulath, K. Mhatre, P.M. Ajayan, S.A. Curley, 3D-Bioprinted inflammation modulating polymer scaffolds for Soft tissue repair, Adv. Mater. 33 (4) (2021), 2003778.
[19] S. Mirel, A. Pusta, M. Moldovan, S. Moldovan, Antimicrobial meshes for hernia repair: Current Progress and Perspectives, J. Clin. Med. 11 (3) (2022) 883.
[20] M. Shokrollahi, S.H. Bahrami, M.H. Nazarpak, A. Solouk, Biomimetic double-sided polypropylene mesh modified by DOPA and ofloxacin loaded carboxyethyl chitosan/polyvinyl alcohol-polycaprolactone nanofibers for potential hernia repair applications, Int. J. Biol. Macromol. 165 (2020) 902–917.
[21] N. Qamar, N. Abbas, M. Irfan, A. Hussain, M.S. Arshad, S. Latif, F. Mehmood, M.U. Ghori, Personalized 3D printed ciprofloxacin impregnated meshes for the management of hernia, J. Drug Deliv. Sci. Technol. 53 (2019), 101164.
[22] L.-M. Zhu, P. Schuster, U. Klinge, Mesh implants: an overview of crucial mesh parameters, World J. Gastrointest. Surg. 7 (10) (2015) 226.
[23] B. Pérez-Köhler, S. Benito-Martínez, V. Gómez-Gil, M. Rodríguez, G. Pascual, J.M. Bellón, New insights into the application of 3D-printing technology in hernia repair, Materials 14 (22) (2021) 7092.
[24] M. Krstić, M. Radojević, D. Stojanović, V. Radojević, P. Uskoković, S. Ibrić, Formulation and characterization of nanofibers and films with carvedilol prepared by electrospinning and solution casting method, Eur. J. Pharmaceut. Sci. 101 (2017) 160–166.
[25] S. Lade Milind, A. Payghan Santosh, J. Tamboli Zaki, I. Disouza John, Polymer based wafer technology: a Review, Int. J. Pharmaceut. Biolog. Archives 4 (6) (2013) 1060–1074.
[26] Z.I. Abdeen, A.F. El Farargy, N.A. Negm, Nanocomposite framework of chitosan/polyvinyl alcohol/ZnO: preparation, characterization, swelling and antimicrobial evaluation, J. Mol. Liq. 250 (2018) 335–343.
[27] M. Fiedot, I. Maliszewska, O. Rac-Rumijowska, P. Suchorska-Woźniak, A. Lewińska, H. Teterycz, The relationship between the mechanism of zinc oxide crystallization and its antimicrobial properties for the surface modification of surgical meshes, Materials 10 (4) (2017) 353.
[28] L. Melman, E. Jenkins, N. Hamilton, L. Bender, M. Brodt, C. Deeken, S. Greco, M. Frisella, B. Matthews, Early biocompatibility of crosslinked and non-crosslinked biologic meshes in a porcine model of ventral hernia repair, Hernia 15 (2) (2011) 157–164.
[29] A. Vandendael, D. Struwig, J. Nel, T. Kruger, C. Lombard, Efficacy of fibrin sealant in prevention of adhesion formation on ovarian surgical wounds in a rabbit model, GynaEcol. Endosc. 5 (3) (1996) 169–172.
[30] E.D. Jenkins, V. Yom, L. Melman, L.M. Brunt, J.C. Eagon, M.M. Frisella, B.D. Matthews, Prospective evaluation of adhesion characteristics to intraperitoneal mesh and adhesiolysis-related complications during laparoscopic re-exploration after prior ventral hernia repair, Surg. Endosc. 24 (12) (2010) 3002–3007.
[31] D.B. Earle, L.A. Mark, Prosthetic material in inguinal hernia repair: how do I choose? Surg. Clin. 88 (1) (2008) 179–201.
[32] S. Idrees, S. Jindal, M. Gupta, R. Sarangi, Surgical meshes–The search continues, Current Med. Res. Pract. 8 (5) (2018) 177–182.
[33] K. Hemalatha, K. Rukmani, N. Suriyamurthy, B. Nagabhushana, Synthesis, characterization and optical properties of hybrid PVA–ZnO nanocomposite: a composition dependent study, Mater. Res. Bull. 51 (2014) 438–446.
[34] S. Keskin, İ. Uslu, T. Tunç, M. Öztürk, A. Aytimur, Preparation and characterization of neodymia doped PVA/Zr-Ce oxide nanocrystalline composites via electrospinning technique, Mater. Manuf. Process. 26 (11) (2011) 1346–1351.
[35] H.S. Mansur, R.L. Oréfice, A.A. Mansur, Characterization of poly (vinyl alcohol)/poly (ethylene glycol) hydrogels and PVA-derived hybrids by small-angle X-ray scattering and FTIR spectroscopy, Polymer 45 (21) (2004) 7193–7202.
[36] K.D. Dejen, E.A. Zereffa, H.A. Murthy, A. Merga, Synthesis of ZnO and ZnO/PVA nanocomposite using aqueous Moringa oleifeira leaf extract template: antibacterial and electrochemical activities, Rev. Adv. Mater. Sci. 59 (1) (2020) 464–476.
[37] D. Yu, Y.Y. Feng, J.X. Xu, B.H. Kong, Q. Liu, H. Wang, Fabrication, characterization, and antibacterial properties of citric acid crosslinked PVA electrospun microfibre mats for active food packaging, Packag. Technol. Sci. 34 (6) (2021) 361–370.
[38] R. Shi, J. Bi, Z. Zhang, A. Zhu, D. Chen, X. Zhou, L. Zhang, W. Tian, The effect of citric acid on the structural properties and cytotoxicity of the polyvinyl alcohol/starch films when molding at high temperature, Carbohydrate polymers 74 (4) (2008) 763–770.
[39] Y. Liu, L.M. Geever, J.E. Kennedy, C.L. Higginbotham, P.A. Cahill, G.B. McGuinness, Thermal behavior and mechanical properties of physically crosslinked PVA/Gelatin hydrogels, J. Mechan. Behav. Biomed. Mater. 3 (2) (2010) 203–209.
[40] A. Chaturvedi, A.K. Bajpai, J. Bajpai, S.K. Singh, Evaluation of poly (vinyl alcohol) based cryogel–zinc oxide nanocomposites for possible applications as wound dressing materials, Mater. Sci. Eng. C 65 (2016) 408–418.
[41] S. Kumaraswamy, G. Babaladimath, V. Badalamoole, S. H Mallaiah, Gamma irradiation synthesis and in vitro drug release studies of ZnO/PVA hydrogel nanocomposites, Adv. Mater. Letters 8 (4) (2017) 546–552.
[42] S. Elango, S. Perumalsamy, K. Ramachandran, K. Vadodaria, Mesh materials and hernia repair, Biomedicine 7 (3) (2017) 14–23.
[43] E. Barua, A.B. Deoghare, S. Chatterjee, P. Sapkal, Effect of ZnO reinforcement on the compressive properties, in vitro bioactivity, biodegradability and cytocompatibility of bone scaffold developed from bovine bone-derived HAp and PMMA, Ceram. Int. 45 (16) (2019) 20331–20345.
[44] P. Feng, P. Wei, C. Shuai, S. Peng, Characterization of mechanical and biological properties of 3-D scaffolds reinforced with zinc oxide for bone tissue engineering, PLoS One 9 (1) (2014), e87755.
[45] M. Mandegari, L. Ghasemi-Mobarakeh, M. Zamani, Manipulating the degradation rate of PVA nanoparticles by a novel chemical-free method, Polym. Adv. Technol. 30 (9) (2019) 2381–2391.
[46] A.M. Neres Santos, A.P. Duarte Moreira, C.W. Piler Carvalho, R. Luchese, E. Ribeiro, G.B. McGuinness, M. Fernandes Mendes, R. Nunes Oliveira, Physically cross-linked gels of PVA with natural polymers as matrices for manuka honey release in wound-care applications, Materials 12 (4) (2019) 559.
[47] A. Das, S. Bhattacharyya, R. Uppaluri, C. Das, Optimality of poly-vinyl alcohol/starch/glycerol/citric acid in wound dressing applicable composite films, Int. J. Biol. Macromol. 155 (2020) 260–272.
[48] X. Liu, X. Chen, J. Ren, M. Chang, B. He, C. Zhang, Effects of nano-ZnO and nano-SiO2 particles on properties of PVA/xylan composite films, Int. J. Biol. Macromol. 132 (2019) 978–986.
[49] M.Q. Khan, D. Kharaghani, S. Ullah, M. Waqas, A.M.R. Abbasi, Y. Saito, C. Zhu, I.S. Kim, Self-cleaning properties of electrospun PVA/TiO2 and PVA/ZnO nanofibers composites, Nanomaterials 8 (9) (2018) 644.
[50] S. Sa'adon, M.N.M. Ansari, S.I.A. Razak, J.S. Anand, N.H.M. Nayan, A.E. Ismail, M.U.A. Khan, A. Haider, Preparation and physicochemical characterization of a diclofenac sodium-dual layer polyvinyl alcohol patch, Polymers 13 (15) (2021) 2459.
[51] D.U. Imaan, F.Q. Mir, B. Ahmad, Synthesis and characterization of a novel poly (vinyl alcohol)-based zinc oxide (PVA-ZnO) composite proton exchange membrane for DMFC, Int. J. Hydrogen Energy 46 (22) (2021) 12230–12241.
[52] R.P. Ten Broek, Y. Issa, E.J. van Santbrink, N.D. Bouvy, R.F. Kruitwagen, J. Jeekel, E.A. Bakkum, M.M. Rovers, H. van Goor, Burden of adhesions in abdominal and pelvic surgery: systematic review and met-analysis, BMJ 347 (2013) f5588.
[53] N. Kakizawa, S. Tsujinaka, Y. Mizusawa, S. Tamaki, R. Maemoto, E. Machida, Y. Muto, M. Saito, N. Toyama, T. Rikiyama, Indications and outcomes of a hybrid method Combining laparoscopic and anterior approaches for inguinal hernia repair, Cureus 14 (7) (2022), e27117.

[54] J. Burger, J. Halm, A. Wijsmuller, S.t. Raa, J. Jeekel, Evaluation of new prosthetic meshes for ventral hernia repair, Surg. Endosc. Other Intervent. Techniq. 20 (8) (2006) 1320–1325.
[55] J. Li, J. Zhu, T. He, W. Li, Y. Zhao, Z. Chen, J. Zhang, H. Wan, R. Li, Prevention of intra-abdominal adhesion using electrospun PEG/PLGA nanofibrous membranes, Mater. Sci. Eng. C 78 (2017) 988–997.
[56] Y.W. Novitsky, A.G. Harrell, J.A. Cristiano, B.L. Paton, H.J. Norton, R.D. Peindl, K.W. Kercher, B.T. Heniford, Comparative evaluation of adhesion formation, strength of ingrowth, and textile properties of prosthetic meshes after long-term intra-abdominal implantation in a rabbit, J. Surg. Res. 140 (1) (2007) 6–11.
[57] S. Barrientos, O. Stojadinovic, M.S. Golinko, H. Brem, M. Tomic-Canic, Growth factors and cytokines in wound healing, Wound Repair Regen. 16 (5) (2008) 585–601.
[58] G.J. Prud'Homme, Pathobiology of transforming growth factor β in cancer, fibrosis and immunologic disease, and therapeutic considerations, Lab. Invest. 87 (11) (2007) 1077–1091.